Structurability: A Collective Measure of the Structural Differences in Vodkas

Naiping Hu,[†] Dan Wu,[†] Kelly Cross,[†] Sergey Burikov,[§] Tatiana Dolenko,[§]
Svetlana Patsaeva,[§] and Dale W. Schaefer*[,†]

[†]Department of Chemical and Materials Engineering, University of Cincinnati, Cincinnati,
Ohio 45221-0012, and [§]Physics Department of Moscow State University, Moscow, 119992 Russia

Although vodka is a reasonably pure mixture of alcohol and water, beverage drinks typically show differences in appeal among brands. The question immediately arises as to the molecular basis, if any, of vodka taste perception. This study shows that commercial vodkas differ measurably from ethanol−water solutions. Specifically, differences in hydrogen-bonding strength among vodkas are observed by ^{1}H NMR, FT-IR, and Raman spectroscopy. Component analysis of the FT-IR and Raman data reveals a water-rich hydrate of composition $E \cdot (5.3 \pm 0.1)H_2O$ prevalent in both vodka and water−ethanol solutions. This composition is close to that of a clathrate−hydrate observed at low temperature, implying a cage-like morphology. A structurability parameter (SP) is defined by the concentration of the $E \cdot (5.3 \pm 0.1)H_2O$ hydrate compared to pure ethanol−water at the same alcohol content. SP thus measures the deviation of vodka from "clean" ethanol−water solutions. SP quantifies the effect of a variety of trace compounds present in vodka. It is argued that the hydrate structure $E \cdot (5.3 \pm 0.1)H_2O$ and its content are related to the perception of vodka.

INTRODUCTION

Vodka is a "tasteless" and colorless spirit drink produced by fermentation and distillation of grain, potatoes, sugar beets, grapes, or cassava (*1*, *2*). Vodka is defined in the United States by the *Code of Federal Regulations* title 27, volume 1, to be: "neutral spirits so distilled, or so treated after distillation with charcoal or other materials, as to be without distinctive character, aroma, taste, or color".

In vodka production, the alcohol obtained from the fermentation and distillation processes undergoes further processing such as passing through charcoal or carbon filters (*2*). The demineralized water, which is filtered through activated carbon and deionization columns (*1*), is of utmost importance. The final product is obtained by blending the rectified spirit and demineralized water in correct proportions, followed by additional filtering before bottling.

The proportion of alcohol in the classic vodka is 40% by volume (U.S. 80 proof). Although Russian vodka with an alcohol content around 40 vol % was introduced at the end of the 17th century (according to the Tsar's edict of 1698), this value is often mistakenly attributed to research completed in 1865 by the eminent Russian chemist Dmitri Mendeleev (*3*). In his doctoral dissertation Mendeleev observed inflection points in the concentration dependence of the density of ethanol−water (E−W) solutions that he attributed to particular hydrate clusters. Mendeleev's work, however, did not affect the legal requirements for vodka.

E−W solutions deviate strongly from ideal mixing behavior. A maximum extent of nonideality was reported near 40 vol % ethanol based on the abnormal physical−chemical properties such as reduced adiabatic compressibility (*4*), negative excess entropy (*5*, *6*), negative excess enthalpies (*7*, *8*), and negative partial volumes (*5*, *9*, *10*). Differential thermal analysis (DTA) and differential scanning calorimetry (DSC) show significant exothermal peaks at 41.7 vol % (17.4 mol %)(*11*) and 37.4 vol % (15.0 mol %)(*12*), corresponding to compositions of $E \cdot 4.75H_2O$ (*11*) and $E \cdot 5.67H_2O$ (*12*), respectively. On the basis of low-temperature X-ray data, researchers have reported peritectic structures $E \cdot 5.67H_2O$ (*13*) and $(6-8)E \cdot 46H_2O$ (*14*), which correspond to 37.4 and 30.3−37.1 vol %, respectively. These volume percentages are in good agreement with the boundaries used in simplified models that divide ethanol−water mixtures into regions (typically water-rich, intermediate, and ethanol-rich). Because ethanol−water solutions cannot be described by a single model over the whole range of concentrations, the transitional concentration dividing the water-rich from intermediate regions is reported to be 17 mol % (*15*) and 20 mol % (*16*), converting to 41.2 and 46.3 vol %, slightly different due to the different techniques used in these studies.

Volume percentage refers to the mixing proportions. For example, a 40 vol % E−W solution is prepared by diluting 40 mL of pure ethanol to a total 100 mL by adding pure water. Due to negative excess volume, the amount of water added is more than 60 mL. Due to different excess volume, the conversion from mole and weight percent to volume percent depends on the ethanol concentration. The factors used for the

*Corresponding author [e-mail dale.schaefer@uc.edu; telephone (513) 556-5431; fax (206) 600-3191].

B *J. Agric. Food Chem.,* Vol. XXX, No. XX, XXXX

Hu et al.

conversion in this study all follow the alcoholometric table given by Thorpe (*17*).

Vodka is an E−W solution blended at the optimal proportion. Perfection, however, is hard to achieve due to the inevitable presence of impurities. Depending on the raw materials and processing protocols, a variety of trace components can be present. These compounds include fusel oils, acetates, and acetic acid (*18*). These compounds are collectively called volatile congeners and are present between 10 and 3000 mg/L in ethanol (*2*). Gas chromatography is generally used to determine the impurity concentrations in vodka (*2, 18*). Ion chromatography to detect anions in vodka was also reported by Lachenmeier et al. (*1*). However, the amount of useful information obtained from chromatography is limited by the design of columns and the setting of injection and chromatographic conditions (*18*). ^{1}H NMR has been used extensively to investigate the hydrogen bonding in distilled spirits and alcohol systems (*19−24*). According to Nose et al. (*21, 22*) impurities such as salts, acids, and phenols strengthen hydrogen bonding in E−W solutions and Japanese sake. We recently reported that the impurity compounds affect ethanol hydration by molecular dynamics simulations (*25*). We can expect that the impurity traces in vodka affect the hydrogen-bonding strength as well.

FT-IR and ion chromatography in combination with multivariate data analysis have been used to authenticate wine and distilled drinks (*26−32*). The multivariate data, however, have not been interpreted from the perspective of structural differences as we propose here.

We compare the structure and hydrogen-bonding (H-bonding) strength of five vodka brands as revealed by density, ^{1}H NMR, FT-IR, and Raman spectroscopy measurements. We introduce a "structurability" parameter, which measures the ability of vodka to sequester water molecules. The structurability of vodka is assessed by a multivariate curve resolution−alternating least squares (MCR-ALS) analysis on FT-IR and Raman spectra. Structurability provides the molecular basis of the differences in vodka formulations as evidenced by the experimental measurements.

MATERIALS AND METHODS

Samples. Four commercial vodka brands, Belvedere (40 vol %), Gray Goose (40 vol %), Skyy (40 vol %), and Stolichnaya (40 vol %), were purchased in the United States. OVAL (42 vol %) was a gift of OVAL Getränkproduktions and Vertriebs GmbH. These vodka samples were used for the ^{1}H NMR and FT-IR measurements. Samples used in the Raman experiment were all purchased in Russia. The ethanol−water solution samples were prepared using a 0.2 *μ*m Millipore hydrophilic PTFE filter (Millipore Corp.) attached to a disposable syringe. The densities of the U.S.-purchased vodkas were obtained using a 50 mL flask and an APX-60 balance (Denver Instruments, Inc.) that has a readability of 0.1 mg. The E−W solutions were prepared by mass using ethanol 200 proof (Pharmco Products, Inc.) and deionized water that was filtered by a Super-Q system (Millipore Corp.). We used absolute, anhydrous, and HPLC grade ethyl alcohol so that the volatile impurities (e.g., methanol, acetal, acetaldehyde, benezene) are all <1 ppm according to the product specification. The ultrapure water used is also adequately pure for this study.

^{1}H NMR, Raman, and FT-IR Measurements. The ^{1}H NMR spectra were obtained using an AMX 400 MHz spectrometer (Bruker Inc.) at 23.2 °C. Me₄Si (TMS) dissolved in deuterated chloroform (Cambridge Isotope Laboratories, Inc.) was used as the external reference to determine the chemical shifts. A sealed capillary tube filled with the TMS solutions was placed in the center of a 5 mm sample tube. The chemical shifts were measured by using the resonance peak of liquid TMS at 23.3 °C as external reference in coaxial tubes as well as by the methyl proton signals of ethyl alcohol. The chemical shifts were evaluated by applying the sideband method (*33, 34*) in repeated measurements. The chemical shifts were then corrected for the volume magnetic susceptibilities of the sample
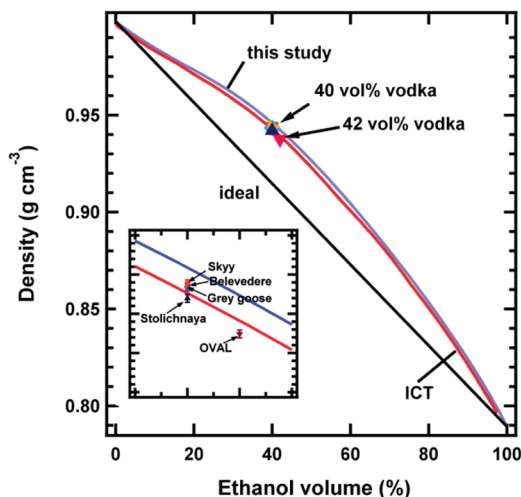

Figure 1. Densities of vodka brands mapped on the density profile measured for ethanol−water solutions (red) in comparison with the values from the International Critical Table (blue) (*44*). Ethanol mole percent for ethanol−water solution samples was converted to volume percent to compare with the standard measure of vodkas. In the inset the region from 40 to 42 vol% is zoomed showing slight differences among vodka brands.

and reference using a method described by Mizuno et al. (*35*). The sample densities used in the method were measured at room temperature.

FT-IR spectra were measured at room temperature in N₂ gas atmosphere using a DigiLab FT-IR/FTS 3000 spectrometer with a DTGS detector (DigiLab, Inc.) with an energy resolution of 0.25 cm⁻¹. A liquid cell with CaF₂ window plates (1 mm path length) separated by a Teflon sheet was used to hold the samples. Contributions from water vapor were removed using internal DigiLab routines. Specifically, a Savitsky−Golay cubic smoothing algorithm was applied to the background-subtracted data except in the region of the sharp C−H asymmetric stretch at 2950 cm⁻¹. Residual water vapor and CO₂ peaks were removed using the built-in "zap" function.

The dependence of water−ethanol solutions can also be obtained from Raman spectra in the region from 200 to 4000 cm⁻¹ (*36*). The Raman experiments were conducted using argon laser radiation (wavelength, 488 nm; power, 450 mW) through the bottom of the quartz cuvette. To control the laser power the beam splitter directed 5% of excitation radiation to a laser power meter (Ophir, model 3-AP). Raman signal scattered at 90° was focused at the entrance slit of the monochromator. A filter (Semrock LP02-488RE) was placed in front of the entrance slit to attenuate elastically scattered radiation at 488 nm by 10⁶ times. The monochromator (Acton, model 2500i, focal distance = 500 mm) has two holographic gratings with 900 and 1800 lines per millimeter. Spectra acquisition was achieved in two modes: consecutive spectra registration by means of a photomultiplier (Hamamatsu H 8259-01) with a photon counting system and parallel spectra registration by means of a CCD camera (Synapse 1024*128 BIUV, Jobin Yvon). In the consecutive registration mode, the widths of entrance and output slits were set to 100 *μ*m, providing spectral resolution of 2 cm⁻¹ (with the use of gratings with 1800 lines per millimeter). In the parallel registration mode, the width of entrance slit was set to 25 *μ*m providing spectral resolution of 2 or 4 cm⁻¹ with the use of gratings with 1800 and 900 lines per millimeter.

MCR-ALS Analysis. MCR-ALS analysis was used to decompose the FT-IR spectra into specific components of different compositions. The MCR-ALS method (*37−41*) follows the general form

$$\mathbf{D} = \mathbf{C}\mathbf{S}^{\mathbf{T}} + \mathbf{E} \qquad (1)$$

In eq 1, **D** is the original FT-IR data matrix, which contains the ethanol solution data (solution mole fraction vs solution FT-IR), **C** is the matrix of pure concentration profiles (solution mole fraction vs hydrate composition), and **S**[T] is the matrix of pure components (hydrate composition vs hydrate FT-IR). **E** is the matrix of residuals. MCR-ALS solves eq 1 iteratively by an alternating least-squares algorithm that calculates **C** and **S**[T] matrices optimally by fitting the experimental data matrix **D**. During

Article

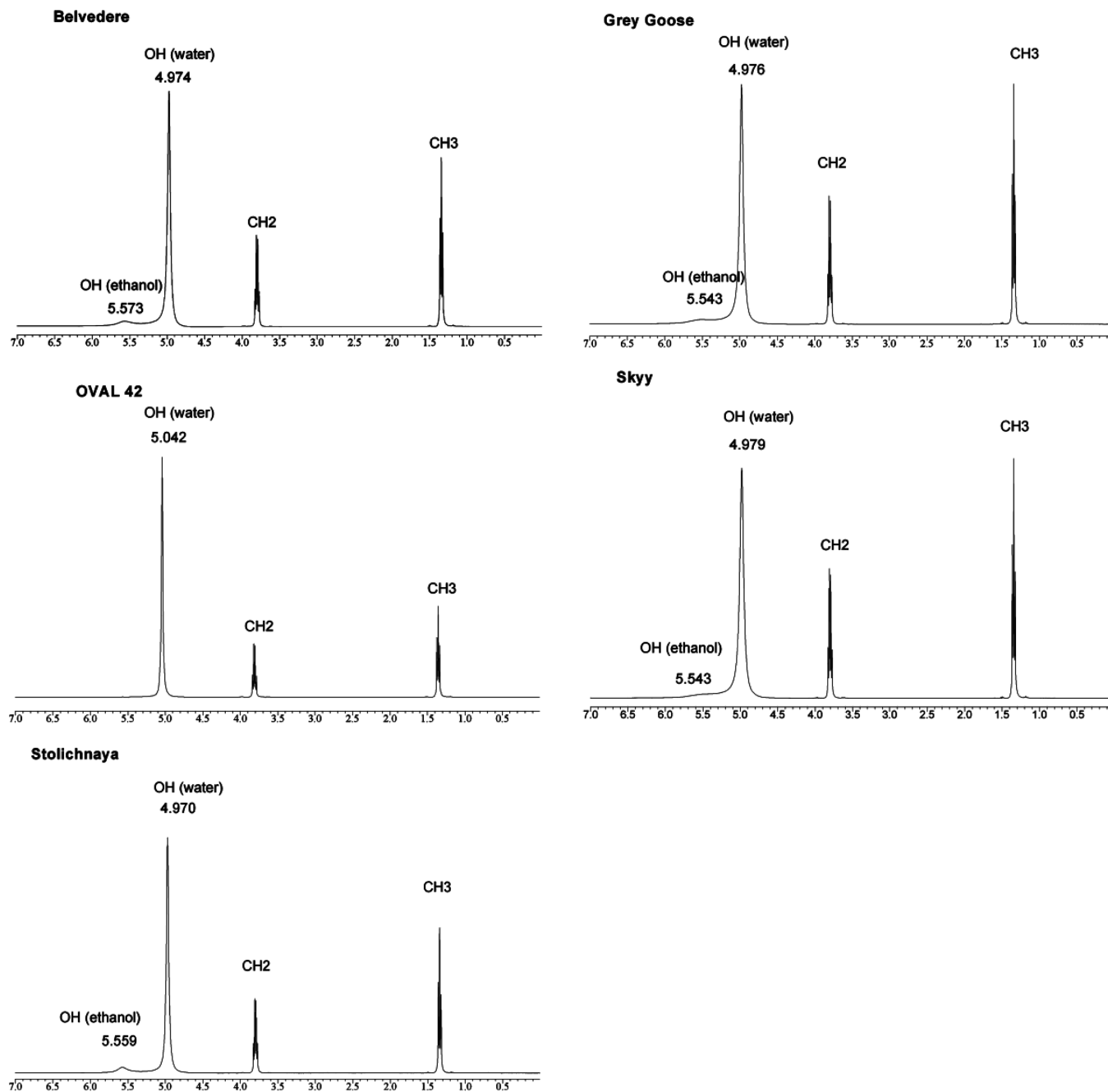*J. Agric. Food Chem.,* Vol. XXX, No. XX, XXXX **C**

Figure 2. ^{1}H NMR spectra of the vodka brands. OVAL shows a coalesced OH peak, whereas the other four vodkas show an individual ethanol−OH peak split from the water peak.

the ALS optimization, non-negativity, unimodality, and closure constraints are applied (*42*). Convergence is achieved when relative differences in standard deviations of the residuals between experimental and ALS calculated values are < 0.1%. The MCR-ALS algorithm implemented by Tauler et al. (*43*) was used to decompose the original FT-IR spectra matrix for E−W solutions into "pure" components and their concentrations. We find that four components are needed to obtain a good fit to the data. The resolved $\mathbf{S^T}$ is used to investigate the cluster structures in vodka by calculating the cluster concentrations, $\mathbf{C_V}$, from

$$\mathbf{C_V} = \mathbf{V(S^T)}^{-1} \tag{2}$$

where $\mathbf{V}$ is the FT-IR data vector for the vodka.

RESULTS AND DISCUSSION

Densities. The densities of the five vodkas are compared with the densities measured for ethanol−water solutions and density

data from the International Critical Table (*44*) in **Figure 1**. As shown, the densities of five vodka products are in good agreement with the values of E−W solutions at their respective volume percentages, all deviating from the ideal mixtures. The densities of four vodkas at 40 vol % are slightly different, suggesting that differences in brands exist at the same nominal alcohol content.

^{1}H NMR, FT-IR, and Raman Measurements. The ^{1}H NMR spectra of five vodkas were measured at 23.2 °C. The raw data were loaded into MestRe-C (MestRe-C, Inc.) to identify the hydroxyl signals using the Peak Picking routine and parabolic interpolation. The chemical shifts were then corrected for the volume magnetic susceptibilities of the sample and reference (*35*). The sample densities were measured at room temperature. As shown in **Figure 2**, the spectra all show a sharp symmetrical hydroxyl signal at a chemical shift of ∼5 ppm corresponding to
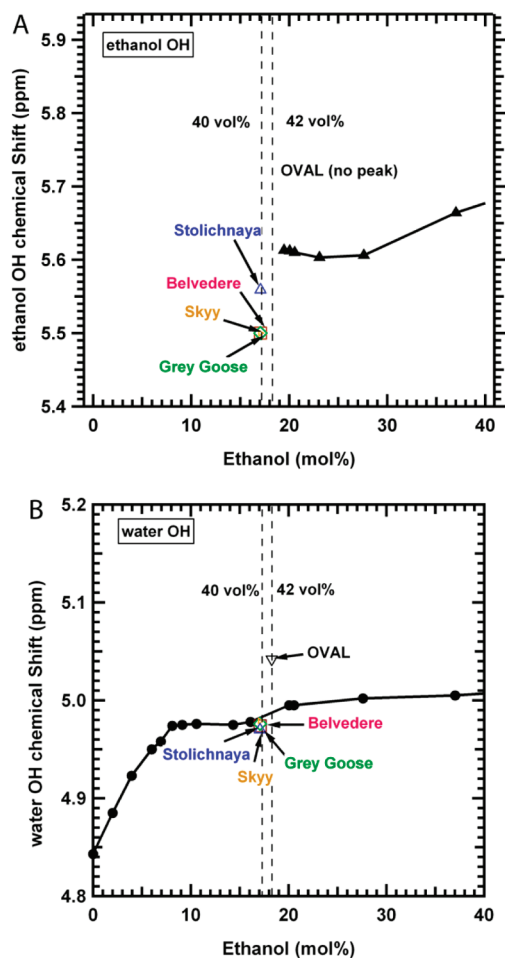
D *J. Agric. Food Chem.,* Vol. XXX, No. XX, XXXX

Hu et al.

Figure 3. ^{1}H NMR chemical shifts of water (**A**) and ethanol (**B**) hydroxyl groups of vodka brands mapped on the ^{1}H NMR chemical shifts of ethanol−water solutions. OVAL deviates from water−ethanol solution in that the water line shifts to the lower field and the ethanol peak is absent. The water OH chemical shifts of Belvedere, Gray Goose, Skyy, and Stolichnaya agree well with that of the 40 vol % ethanol−water solution. The ethanol OH, however, emerges as an individual peak, deviating from the trend shown in (**B**) for ethanol−water solutions. It is interesting that although OVAL has a higher ethanol content (42 vol %), it shows no ethanol peak, whereas the other brands do show an ethanol peak even though they have lower ethanol content (40 vol %).

hydroxyl groups in water. This OH signal is shifted downfield in the following order: Stolichnaya, Belvedere, Gray Goose, Skyy, OVAL. The spectra also show a second signal at ∼5.5 ppm for all brands except OVAL. Especially for Belvedere and Stolichnaya, the low-field peaks are split from the high-field OH signals at ∼5 ppm, with an independent maximum emerging. The secondary peaks are broad, and so the peak's chemical shift was identified as the position where a maximum height was observed from the peak list after Peak Picking was performed.

The results of chemical shifts of the water and ethanol protons with respect to external reference TMS are mapped onto the chemical shift plot of E−W solutions (*45*) in **Figure 3**. As shown in **Figure 3A**, a critical ethanol concentration is observed at 20 mol % (46.3 vol %) for E−W solutions. The resonance peaks of the water protons and the alcohol OH proton coalesce into a single peak below the critical concentration; above 20 mol % ethanol, the signals from water and ethanol split. The four vodkas at 40 vol % (slightly lower than the critical concentration 46.3 vol %) surprisingly all show individual peaks for the ethanol
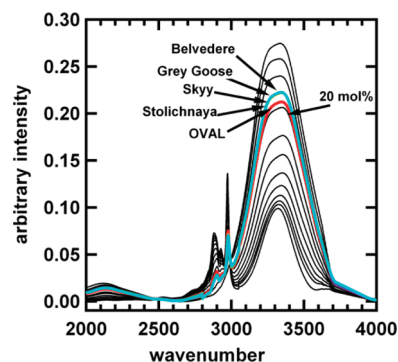

Figure 4. FT-IR spectra of vodka brands (colored) in comparison with the FT-IR data obtained for ethanol−water solutions (black). The data for Belvedere, Gray Goose, Skyy, and Stolichnaya overlap with that for a 20 mol % ethanol−water solution in the range from 3000 to 3500 cm^{-1}. Other bands differ for all samples. The intensity of the O−H stretching band (3000−3500 cm^{-1}) for ethanol−water solutions (black lines) decreases as ethanol mole fraction increases.
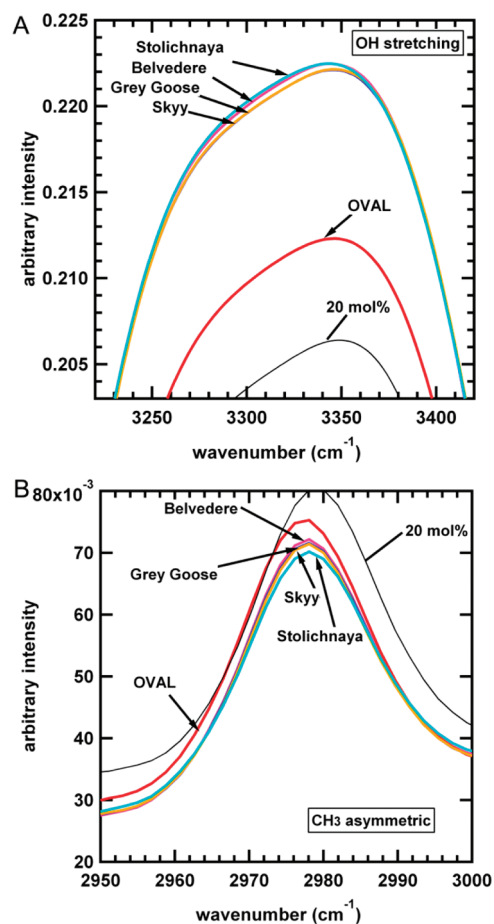

Figure 5. FT-IR (**A**) O−H stretching band and (**B**) asymmetric CH$_3$ stretching band of vodka brands compared with data for 20 mol % ethanol−water solutions. OVAL (42 vol %) is significantly different from other vodka brands (40 vol %). All vodka data deviate from that of a 20 mol % (46 vol %) ethanol−water solution.

hydroxyl groups. By contrast, OVAL at 42 vol % shows only one coalesced peak. The absence of an ethanol OH signal in OVAL implies weaker ethanol H-bonding compared to the other brands so that the ethanol-like environment in OVAL was not detected as an individual peak in the NMR spectra. In addition, as shown in **Figure 3B**, OVAL deviates from water−ethanol solution and
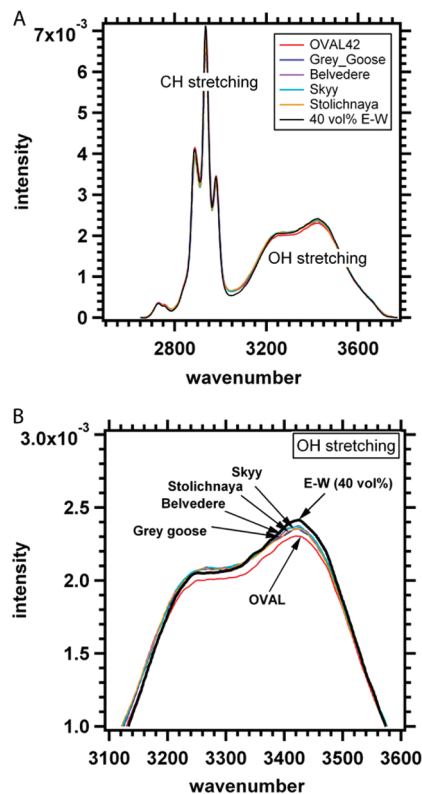
Article

J. Agric. Food Chem., Vol. XXX, No. XX, XXXX **E**

Figure 6. Raman spectra of vodka brands in the regions of (**A**) CH and OH stretching bands and (**B**) enlarged OH stretching band. In (**A**), the CH and OH stretchings of all vodkas are similar to those of the pure ethanol–water solutions (40 vol %). However, in (**B**), the enlarged OH stretching region shows that OVAL differs measurably from other vodka products.

Figure 7. Four-component analysis of IR spectra giving the resolved "pure" components (**A**) and their concentration profiles (**B**). The components are identified as water, E·5.36H$_2$O, E·1.28H$_2$O, and ethanol (*45*).

other vodkas in that the water line shifts to the lower field, suggesting stronger water H-bonding (*21, 22*).

The difference in O–H stretching bands among vodkas was also studied by the FT-IR and Raman spectroscopy (**Figures 4–6**). As shown by the FT-IR spectra in **Figure 5**, both the O–H and C–H stretching bands of vodkas deviate from the pure E–W solution at 20 mol % (46 vol %). The 20 mol % E–W solution is the experimental sample closest to the nominal vodka percentage (40 vol %). The broad O–H stretching bands of vodkas (**Figure 5A**) differ only modestly among themselves except for OVAL. This deviation may be attributed to a slightly higher volume percentage of OVAL (42 vol %) than the other brands (40 vol %). The asymmetric CH$_3$ stretching bands of vodkas differ more significantly between vodkas and the 20 mol % E–W solution. OVAL also shows deviation from both other vodka brands and the 20 mol % E–W solution.

The C–H and O–H stretching bands of the Raman spectra for vodkas are compared with those of 40 vol % E–W solution in **Figure 6**. Except for OVAL the data differ slightly from those of pure E–W solutions (**Figure 6A**). However, in **Figure 6B**, OVAL shows different OH stretching bands from all other vodkas due to its slightly higher ethanol content (42 vol %).

The ^{1}H NMR results indicate increased H-bonding in OVAL as shown by the downfield chemical shift of the water OH signal. The enhanced H-bonding structures could be due to structural differences introduced by traces of a variety of impurity compounds. The structural effect of impurity compounds is a complicated matter that depends on both geometric and electrostatic properties of the compounds (*25*). Also, multiple impurities in small quantities could have a collective impact on properties. To
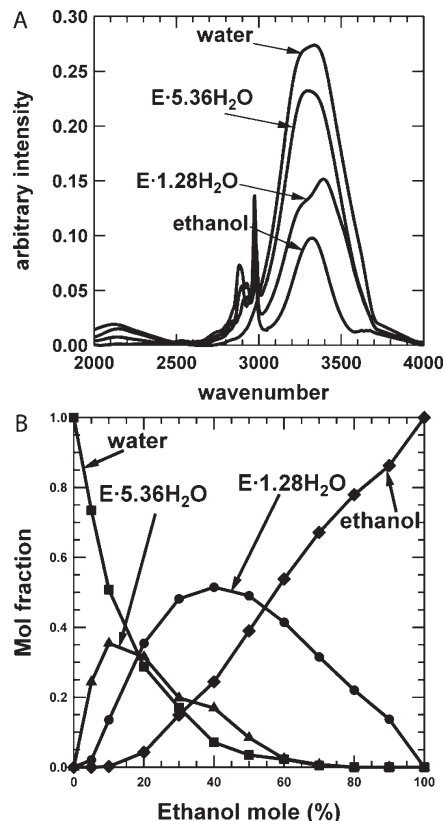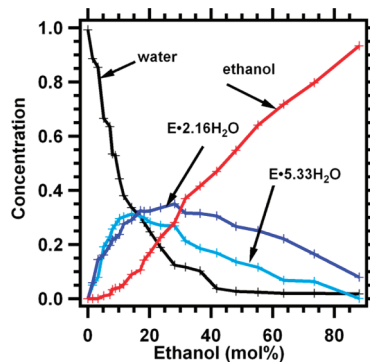

Figure 8. Concentration profiles of the four-component analysis results of Raman spectra. The components are identified as water, E·5.33H$_2$O, E·2.16H$_2$O, and ethanol.

quantify the collective effect we propose a MCR-ALS approach to explore the structural basis of the differences in vodka.

MCR-ALS Analysis. Our approach is based on a four-component MCR-ALS analysis of the FT-IR spectra of E–W solutions (in the range from 2000 to 4000 cm^{-1}). The computational details can be found elsewhere (*45*). The results on the resolved FT-IR spectra (**S^T**) and the concentrations (**C**) are shown in **Figure 7**. By comparing the resolved spectra (**Figure 7A**) to the spectra of E–W solutions, the "pure" components have been identified as water, ethanol hydrate 1 (E·5.36H$_2$O), ethanol hydrate 2 (E·1.28H$_2$O), and ethanol (*45*). The same approach applied to the Raman data yields similar results (hydrate structures of E·5.33H$_2$O and E·2.16H$_2$O) as shown in **Figure 8**. The FT-IR and Raman analyses agree on the composition of the first hydrate, E·(5.3 ± 0.1)H$_2$O. The second hydrate has a composition
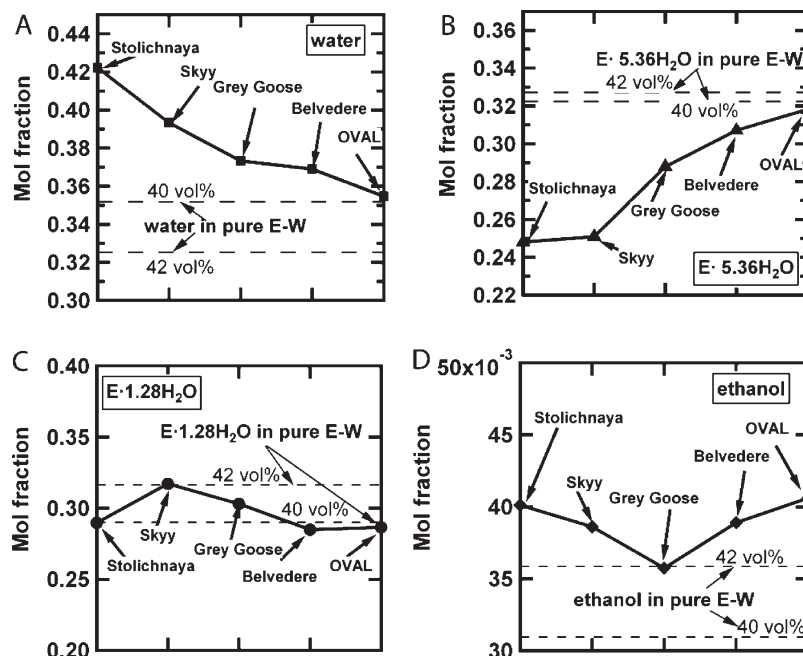
Figure 9. Mole fractions of water (**A**), ethanol hydrate E·5.36H$_2$O (**B**), E·1.28H$_2$O (**C**), and ethanol (**D**) in vodka brands based on IR spectra. The concentrations are compared with those of 40 and 42 vol % ethanol−water (E−W) solutions as shown by horizontal dashed lines. OVAL has the least water clusters but the most water-rich ethanol hydrate structures. The values for water and E·5.36H$_2$O for the 40 and 42 vol % "clean" solutions (horizontal lines) are of particular importance as they are used in the calculation of the structurability parameter in **Figure 11**. These values were obtained by interpolation from the values based on experimental samples (10 and 20 mol % corresponding to 27 and 46 vol %, respectively).

of E·(1.8 ± 0.5H$_2$O). Both hydrates are transient cluster structures related to E−W crystals at low temperature.

To investigate the cluster structures in vodka, we used the FT-IR data of commercial brands shown in **Figure 4**. Substituting **S^T** and vodka FT-IR results (data in **Figure 4**) into eq 2, we obtained the component concentrations (**C$_V$**) in five vodkas as compared in **Figure 9**.

The pure ethanol component concentration is comparable in all vodka brands and close to zero, indicating no significant amount of ethanol−ethanol clusters are present. The concentration of the first hydrate E·5.3H$_2$O in OVAL is the highest among the vodkas, whereas the water concentration is the lowest. The results imply that H-bonding is strengthened between E−W clusters of composition E·5.3H$_2$O. The high content of E·5.3H$_2$O compensates for the decrease of water−water clusters, leading to a coalesced water OH peak in the NMR spectrum of OVAL. Comparison with E−W solutions (dashed horizontal lines) shows that the water component is enhanced (**Figure 9A**) and the E·5.36H$_2$O component is diminished (**Figure 9B**) in all vodka products.

The E·5.3H$_2$O hydrate can be identified as a relative of clathrate I observed at low temperature. It was determined from the lattice data for 6E·46H$_2$O, which is a cubic clathrate I with a unit cell of 12.03 Å and space-group symmetry *Pm3n* (*14*). The ethanol hydrate crystal structure is not available, so we constructed a unit cell from the similar *Pm3n* ethylene oxide hydrate (clathrate I) reported by McMullan et al. (*46*). Ethylene oxide molecules were then replaced with ethanol molecules in the unit cell to represent ethanol hydrate clathrate consisting of 6 ethanol and 46 water molecules. A supercell with a lattice constant of 36.09 Å was constructed from the unit cell and then subjected to 5000 steps of minimization. The final structure has a cell constant of 37.25 Å. The cubic unit cell of 12.03 Å with space-group symmetry *Pm3n* is shown in **Figure 10A**. The side view of the supercell, which consists of 27 unit cells, is shown in **Figure 10B**, revealing the water cages with ethanol molecules captured in the cages. Due to lack of crystallographic data for E−W, these cells

that we constructed based on similar ethylene oxide crystal are only approximation for visualization. However, we propose that in E−W solutions, similar caged cluster structures (E·5.3H$_2$O) exist as short-lived disordered entities, mixed with water−water, ethanol−ethanol, and E·1.8H$_2$O clusters.

Structurability Parameter (SP). The content of the water-rich hydrate (mole fraction of E·5.3H$_2$O, or X_{E-W}) can be used as a collective measure of structural differences among vodkas. By decomposing the FT-IR spectra into discrete cluster entities and obtaining the X_{E-W} values, component analysis provides a structural basis to interpret the H-bonding characteristics observed by ^{1}H NMR, FT-IR, and Raman.

We define a structurability parameter (SP) as the mole ratio of water-rich ethanol hydrate (X_{E-W}) to water (X_{W-W}) normalized by the ratio in pure ethanol−water solutions at the same ethanol content

$$\text{SP} = \frac{(X_{E-W}/X_{W-W})_{\text{vodka}}}{(X_{E-W}/X_{W-W})_{E-W \text{ solution}}} \quad (3)$$

SP therefore measures the deviation of vodka from pure E−W solutions in terms of propensity to form the E·5.3H$_2$O hydrate. The lower the value of SP, the more significant the deviation from the pure solution. The SPs for the vodkas are shown in **Figure 11**. Ethanol hydrate and water content (X_{E-W} and X_{W-W}) obtained on the 42 vol % E−W solution were used to calculate the SP value for OVAL, whereas X_{E-W} and X_{W-W} from the 40 vol % E−W solution were used for the SPs of four other samples. Stolichnaya deviates most significantly from the pure 40 vol % E−W solution. OVAL shows the highest extent of E·5.3H$_2$O formation and the lowest water component.

We have noted that the vodka samples used in FT-IR and Raman were purchased in the United States and Russia, respectively. Because of possible differences in vodka meant for different markets, the structurability parameter analysis in this study is based on the FT-IR data for vodka purchased in United States.
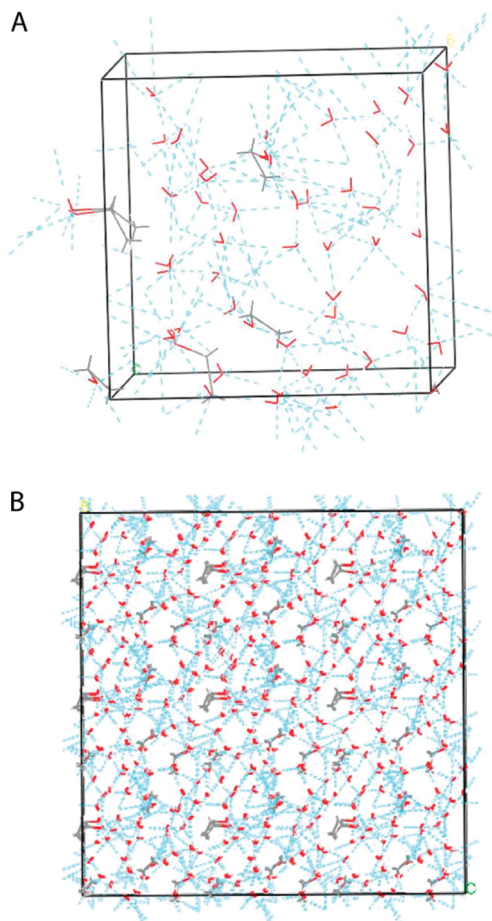
A

B

Figure 10. 3D view of the unit cell (**A**) and side view of the supercell of the ethanol clathrate $E \cdot 5.36H_2O$ (**B**). The water forming the cages and ethanol molecules captured in the cages are represented by solid lines. The blue lines are hydrogen bonds between H-bonded molecules. The cell length is 12.03 Å for the unit cell and 37.25 Å for the supercell.

Figure 11. The structurability parameters (SPs) of vodka brands calculated by eq 3. Stolichnaya has the lowest SP value and thus deviates the most from a "clean" E−W solution.

In conclusion, the difference among vodkas is revealed by ^{1}H NMR, FT-IR, and Raman spectroscopy. We demonstrated a new approach based on component analysis of FT-IR and Raman spectra to correlate observed spectral data with H-bonded transient structures. The structurability of vodka is then characterized by the ratio of $E \cdot (5.3 \pm 0.1)H_2O$ to water (X_{E-W}/X_{W-W}) (X_{W-W}), which collectively represents the deviation of the vodka from clean E−W solutions.

We began this discussion with the statement that vodka is a colorless, tasteless water−ethanol solution. So how do vodka drinkers develop brand preference? Our answer is structure. Beverages with low structurability are likely to be perceived as watery, because the fraction of water clusters is higher than in brands with high structurability. Beverages with high structurability, on the other hand, harbor transient cage-like entities where the ethanol molecule is sequestered by surrounding water molecules. At high alcohol content (above ∼19 mol % or ∼44 vol %) clusters of alcohol molecules appear, as revealed by the emergence of the ethanol line in 400 MHz NMR (**Figure 3**). These ethanol clusters undoubtedly stimulate the palate differently from either water or the $E \cdot 5.3H_2O$ cage structure. Even in the absence of "taste" in the traditional sense, vodka drinkers could express preference for a particular structure.

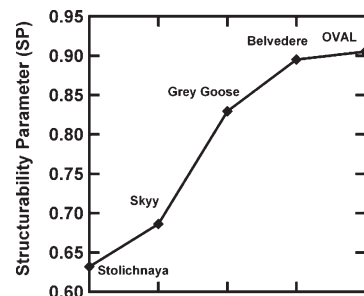Why do vodkas differ in structurability? Although we did not address this issue specifically, one possibility is that trace impurity compounds influence H-bonding and thus alter the component distribution. We are currently investigating this issue using computer simulation. An important conclusion of these studies is that the proposed clathrate structure for the $E \cdot 5.3H_2O$ is transient in nature. Long-lived clusters are not present in liquids that are remote from phase boundaries.

It is interesting to note that $E \cdot 5.3H_2O$ component is significant at a composition of 40 vol %, which is close to the nominal vodka alcohol content. This volume percent is also slightly below the composition where pure ethanol clusters are observed by 400 MHz NMR. At this composition, both "pure" water and "pure" alcohol clusters are dominated by $E \cdot 5.3H_2O$. It seems then that after almost two centuries we may have stumbled upon a molecular basis for early Russian vodka standards.

LITERATURE CITED

(1) Lachenmeier, D. W.; Attig, R.; Frank, W.; Athanasakis, C. The use of ion chromatography to detect adulteration of vodka and rum. *Eur. Food Res. Technol.* **2003**, *218* (1), 105–110.

(2) Ng, L. K.; Hupe, M.; Harnois, J.; Moccia, D. Characterisation of commercial vodkas by solid-phase microextraction and gas chromatography mass spectrometry analysis. *J. Sci. Food Agric.* **1996**, *70* (3), 380–388.

(3) Mendeleev, D. I. *Solutions* (*in Russian*); Izd. Akad. Nauk SSSR: Moscow, Russia, 1959.

(4) Onori, G. Adiabatic compressibility and structure of aqueous-solutions of ethyl-alcohol. *J. Chem. Phys.* **1988**, *89* (7), 4325–4332.

(5) Franks, H. S.; Evans, M. W. Free volume and entropy in condensed systems III. entropy in binary liquid mixtures; partial molar entropy in dilute solutions; structure and thermodynamics in aqueous electrolytes. *J. Chem. Phys.* **1945**, *13*, 507–532.

(6) Petong, P.; Pottel, R.; Kaatze, U. Water−ethanol mixtures at different compositions and temperatures. A dieletric relaxation study. *J. Phys. Chem. A* **2000**, *104* (32), 7420–7428.

(7) Ott, J. B.; Stouffer, C. E.; Cornett, G. V.; Woodfield, B. F.; Wirthlin, R. C.; Christensen, J. J.; Deiters, U. K. Excess-enthalpies for (ethanol + water) at 298.15-K and pressures of 0.4, 5, 10, and 15 MPa. *J. Chem. Thermodyn.* **1986**, *18* (1), 1–12.

(8) Wormald, C. J.; Lloyd, M. J. Excess enthalpies for (water plus ethanol) at $T = 398$ K to $T = 548$ K and $p = 15$ MPa. *J. Chem. Thermodyn.* **1996**, *28* (6), 615–626.

(9) Mitchell, A. G.; Wynne-Jones, W. F. K. *Discuss. Faraday Soc. Art.* **1953**, *15*, 161.

(10) Ott, J. B.; Sipowska, J. T.; Gruszkiewicz, M. S.; Woolley, A. T. Excess volumes for (ethanol plus water) at the temperatures (298.15 and 348.15)K and pressures (0.4, 5, and 15) MPa and at the temperature 323.15-K and pressures (5 and 15) MPa. *J. Chem. Thermodyn.* **1993**, *25* (2), 307–318.

(11) Zelenin, Y. M. Effect of pressure on clathrate formation in a water−ethanol system. *J. Struct. Chem.* **2003**, *44* (1), 130–136.

(12) Takaizumi, K.; Wakabayashi, T. The freezing process in methanol−, ethanol−, and propanol−water systems as revealed by differential scanning calorimetry. *J. Solution Chem.* **1997**, *26* (10), 927–939.

H *J. Agric. Food Chem.,* Vol. XXX, No. XX, XXXX

Hu et al.

(13) Takamuku, T.; Saisho, K.; Nozawa, S.; Yamaguchi, T. X-ray diffraction studies on methanol−water, ethanol−water, and 2-propanol−water mixtures at low temperatures. *J. Mol. Liq.* **2005**, *119* (1−3), 133–146.

(14) Boutron, P.; Kaufmann, A. Metastable states in the system water−ethanol. Existence of a second hydrate; curious properties of both hydrates. *J. Chem. Phys.* **1978**, *68* (11), 5032–5041.

(15) Koga, Y.; Nishikawa, K.; Westh, P. "Icebergs" or no "icebergs" in aqueous alcohols?: composition-dependent mixing schemes. *J. Phys. Chem. A* **2004**, *108* (17), 3873–3877.

(16) Noskov, S. Y.; Lamoureux, G.; Roux, B. Molecular dynamics study of hydration in ethanol−water mixtures using a polarizable force field. *J. Phys. Chem. B* **2005**, *109* (14), 6705–6713.

(17) Thorpe, T. E. S. *Alcoholometric Tables*; Longsmans, Green: London, U.K., 1915.

(18) MacNamara, K.; Leardi, R.; Sabuneti, A. Fast GC analysis of major volatile compounds in distilled alcoholic beverages − optimisation of injection and chromatographic conditions. *Anal. Chim. Acta* **2005**, *542* (2), 260–267.

(19) Akahoshi, R.; Ohkuma, H. Studies on aged spirits and their physicochemical characteristics.1. NMR-spectra of hydroxyl protons in aged spirits. *J. Agric. Chem. Soc. Jpn.* **1984**, *58* (4), 357–365.

(20) Nose, A.; Hamasaki, T.; Hojo, M.; Kato, R.; Uehara, K.; Ueda, T. Hydrogen bonding in alcoholic beverages (distilled spirits) and water−ethanol mixtures. *J. Agric. Food Chem.* **2005**, *53* (18), 7074–7081.

(21) Nose, A.; Hojo, M.; Ueda, T. Effects of salts, acids, and phenols on the hydrogen-bonding structure of water−ethanol mixtures. *J. Phys. Chem. B* **2004**, *108* (2), 798–804.

(22) Nose, A.; Myojin, M.; Hojo, M.; Ueda, T.; Okuda, T. Proton nuclear magnetic resonance and Raman spectroscopic studies of Japanese sake, an alcoholic beverage. *J. Biosci. Bioeng.* **2005**, *99* (5), 493–501.

(23) Okouchi, S.; Ishihara, Y.; Ikeda, S.; Uedaira, H. Progressive increase in minimum proton exchange rate with maturation of liquor. *Food Chem.* **1999**, *65* (2), 239–243.

(24) Price, W. S.; Ide, H.; Arata, Y. Solution dynamics in aqueous monohydric alcohol systems. *J. Phys. Chem. A* **2003**, *107* (24), 4784–4789.

(25) Hu, N.; Schaefer, D. W. Effect of impurity compounds on ethanol hydration. *J. Mol. Liq.* **2010** (doi:10.1016/j.molliq.2010.05.001).

(26) Arvanitoyannis, I. S.; Katsota, M. N.; Psarra, E. P.; Soufleros, E. H.; Kallithraka, S. Application of quality control methods for assessing wine authenticity: use of multivariate analysis (chemometrics). *Trends Food Sci. Technol.* **1999**, *10* (10), 321–336.

(27) Lachenmeier, D. W. Rapid quality control of spirit drinks and beer using multivariate data analysis of Fourier transform infrared spectra. *Food Chem.* **2007**, *101* (2), 825–832.

(28) Lachenmeier, D. W.; Richling, E.; Lopez, M. G.; Frank, W.; Schreier, P. Multivariate analysis of FTIR and ion chromatographic data for the quality control of tequila. *J. Agric. Food Chem.* **2005**, *53* (6), 2151–2157.

(29) Moreira, J. L.; Santos, L. Spectroscopic interferences in fourier transform infrared wine analysis. *Anal. Chim. Acta* **2004**, *513* (1), 263–268.

(30) Palma, M.; Barroso, C. G. Application of FT-IR spectroscopy to the characterisation and classification of wines, brandies and other distilled drinks. *Talanta* **2002**, *58* (2), 265–271.

(31) Patz, C. D.; Blieke, A.; Ristow, R.; Dietrich, H. Application of FT-MIR spectrometry in wine analysis. *Anal. Chim. Acta* **2004**, *513* (1), 81–89.

(32) Picque, D.; Lieben, P.; Corrieu, G.; Cantagrel, R.; Lablanquie, O.; Snakkers, G. Discrimination of cognacs and other distilled drinks by mid-infrared spectropscopy. *J. Agric. Food Chem.* **2006**, *54* (15), 5220–5226.

(33) Arnold, J. T.; Packard, M. E. *J. Chem. Phys.* **1951**, *19*, 1608.

(34) Huggins, M.; Pimentel, G. C.; Shoolery, J. N. *J. Chem. Phys.* **1955**, *23*, 1244.

(35) Mizuno, K.; Kimura, Y.; Morichika, H.; Nishimura, Y.; Shimada, S.; Maeda, S.; Imafuji, S.; Ochi, T. Hydrophobic hydration of *tert*-butyl alcohol probed by NMR and IR. *J. Mol. Liq.* **2000**, *85* (1−2), 139–152.

(36) Burikov, S. A.; Dolenko, T. A.; Patsaeva, S. V.; Yuzhakov, V. I. Diagnostics of aqueous ethanol solutions using Raman spectroscopy. *Atmos. Oceanic Opt.* **2009**, *22* (11), 1082–1088.

(37) Mendieta, J.; DiazCruz, M. S.; Tauler, R.; Esteban, M. Application of multivariate curve resolution to voltammetric data. 2. Study of metal-binding properties of the peptides. *Anal. Biochem.* **1996**, *240* (1), 134–141.

(38) Nigam, S.; de Juan, A.; Cui, V.; Rutan, S. C. Characterization of reversed-phase liquid chromatographic stationary phases using solvatochromism and multivariate curve resolution. *Anal. Chem.* **1999**, *71* (22), 5225–5234.

(39) Salau, J. S. I.; Tauler, R.; Bayona, J. M.; Tolosa, I. Input characterization of sedimentary organic contaminants and molecular markers in the Northwestern Mediterranean Sea by exploratory data analysis. *Environ. Sci. Technol.* **1997**, *31* (12), 3482–3490.

(40) Tauler, R.; Kowalski, B.; Fleming, S. Multivariate curve resolution applied to spectral data from multiple runs of an industrial-process. *Anal. Chem.* **1993**, *65* (15), 2040–2047.

(41) Vives, M.; Gargallo, R.; Tauler, R. Study of the intercalation equilibrium between the polynucleotide poly(adenylic)-poly(uridylic) acid and the ethidium bromide dye by means of multivariate curve resolution and the multivariate extension of the continuous variation and mole ratio methods. *Anal. Chem.* **1999**, *71* (19), 4328–4337.

(42) Saurina, J.; Hernandez-Cassou, S.; Tauler, R. Multivariate curve resolution applied to continuous-flow spectrophotometric titrations - reaction between amino-acids and 1,2-naphthoquinone-4-sulfonic acid. *Anal. Chem.* **1995**, *67* (20), 3722–3726.

(43) Tauler, R.; de Juan, A. *Multivariate Curve Resolution-Alternating Least-Squares* (*MCR-ALS*)*, MatLab Code*; University of Barcelona: Barcelona, Spain, 1999.

(44) Washburn, E. W.; West, C. J.; Dorsey, N. E. National Research Council (U.S.); International Research Council.; National Academy of Sciences (U.S.); Knovel (Firm), International critical tables of numerical data, physics, chemistry, and technology. In *Knovel Scientific and Engineering Databases*, 1st electronic ed.; Knovel: Norwich, NY, 2003.

(45) Hu, N.; Wu, D.; Cross, K. J.; Schaefer, D. W. Structural basis of the ^{1}H NMR spectrum of ethanol−water solutions based on multivariate curve resolution analysis of mid-IR spectrum. *J. Appl. Spectrosc.* **2010**, *64* (3), 337–342.

(46) McMullan, R. K.; Jeffrey, G. A. Polyhedral clathrate hydrates. IX. Structure of ethylene oxide hydrate. *J. Chem. Phys.* **1965**, *42* (8), 2725–2732.